J Mater Sci (2015) 50:4115–4121
DOI 10.1007/s10853-015-8967-3

Synthesis of octahedral and cubic Cu_2O microcrystals in sub- and super-critical methanol and their photocatalytic performance

Shuangming Li[1,2] · Xin Ge[1] · Shengnan Jiang[1] · Xiaona Peng[3] · Zhe Zhang[1] · Wenxiu Li[1,2] · Sansan Yu[1,2]

Received: 19 January 2015 / Accepted: 10 March 2015 / Published online: 20 March 2015

Abstract A simple and potentially scalable sub- and super-critical methanol technique was applied to synthesize cuprous oxide. Cu_2O microcrystals with two morphologies were obtained in methanol of subcritical domain by adjusting the feeding methods. The effects of the reaction time, temperature, pressure, and feeding method on the formation of Cu_2O microcrystals were investigated. XRD, SEM, and XPS were applied to analyze the composition and morphology of products. Results showed that pure cuprous oxide could be obtained in subcritical methanol of 230 °C, 7.8 MPa for 15 min. The two as-obtained products displayed octahedral and cubic morphology with an average edge length of 4 and 2 μm by solution and solid feeding methods, respectively. The formation and crystal growth mechanism of Cu_2O in subcritical methanol were also proposed on the basis of above results. Furthermore, the two microcrystals were employed as catalysts in the photodecomposition of negatively charged molecule methyl orange. Results showed that both microcrystals possessed excellent photocatalytic activities. However, the obvious difference between cubic and octahedral in photocatalytic performance was not found in the scale of micrometer (2–4 μm).

✉ Sansan Yu
ssyu@syuct.edu.cn

Shuangming Li
lishuangming@syuct.edu.cn

Xin Ge
gexin6875093@126.com

Shengnan Jiang
13889827175@163.com

Xiaona Peng
syuctlinchan@126.com

Zhe Zhang
zhangzhezhanghe@hotmail.com

Wenxiu Li
wxli@syict.edu.cn

[1] College of Chemical Engineering, Shenyang University of Chemical Technology, No.9, 11St., Shenyang Economic & Technological Development Zone, Shenyang 110142, China

[2] Key Laboratory of Chemical Separation Technology of Liaoning Province, Shenyang University of Chemical Technology, Shenyang 110142, China

[3] Guangdong Food and Drug Vocational and Technical School, Guangzhou 501163, China

Introduction

Cu_2O, with a bulk direct band-gap energy of 2.17 eV, is an attractive p-type semiconductor [1]. It has attracted much interest recently due to its excellent catalytic, electrical, sensing, and conductive properties and has been widely applied in various fields, including organic synthesis [2–4], photocatalysis [5–7], solar energy conversion [8], gas sensors [9, 10], lithium ion batteries [11–13], antibacterial [14, 15], and often used as hybrid by compounding with other materials [16–19].

To date, the synthetic strategies of Cu_2O nano/micro particles have been developed by many researchers, and various morphologies have been obtained. Among them, the wet chemical approach was the most commonly used method. For instance, the Huang group synthesized Cu_2O nanocubes, octahedra, octapods, rhombic dodecahedron, edge- and corner-truncated octahedron, truncated rhombic dodecahedron, etc., by using aqueous solution reduction methods [3, 20–23]. Xu et al. used ascorbic acid as the reducing agent and beta-cyclodextrin as the capping agent

to prepare porous Cu_2O nanospheres via a sonochemical route [24]. Zhang et al. obtained Cu_2O hollow spheres with thin shells in deionized water by using poly(vinylpyrrolidone) as the template, in which, $CuAc_2{\cdot}H_2O$ was reduced by ascorbic acid in the presence of PVP and sodium hydroxide [25]. Jin et al. fabricated Cu_2O nanowires and nanotubes by reducing Cu^{2+} with glucose or fructose via Fehling's reaction [26]. In addition, solvothermal [5, 6, 15, 27] was also often applied to synthesize various interesting cuprous oxide.

In these above reported methods, the morphologies of cuprous oxide nano/micro particles could be easily controlled by adjusting the amount of reductants and surfactants, the introduction order of the reagents, and the reaction time. However, a very complex reaction system consisting of solvent, precursor, reducing agent, surfactant, stabilizer, and other additives was required in these methods. Moreover, these methods were not environmentally friendly due to the usage of toxic agents and expensive organic compounds, which were the major drawbacks for industrial application. Thus, it is urgent to develop a simple, environmentally friendly, and scalable methodology for the synthesis of cuprous oxide.

In recent years, the synthesis of metal oxide nano/micro particles in sub- and super-critical fluids has been extensively reported. Due to the advantages of possessing adjustable physical properties, being environmentally benign and avoiding the usage of toxic and expensive chemical agents, sub- and super-critical fluids have been considered as a promising alternative method for fabricating fine metal-based materials. So far, various metal-based nano/micro particles have been synthesized in sub- and supercritical fluids, such as metal (Cu, Ni, Ag, Co, Au, Pd, Pt) [28–34], metal oxides (Al_2O_3, TiO_2, Ga_2O_3, CeO_2, Fe_3O_4, ZnO, In_2O_3, Mn_3O_4, Gd_2O_3, Eu_3O_3, Nd_2O_3, CuO, Fe_2O_3, NiO, ZrO_2) [31, 32, 35–41], composite metal oxides ($BaTiO_3$, $MnFe_2O_4$, $Li_4Ti_5O_{12}$, $LiFePO_4$, $LiFePO_4$) [42–45], metal nitride (Cr_2N, Co_2N, Fe_4N, Cu_3N, Ni_3N) [32], metal sulfide (ZnS, CdS, PbS) [31], and selenides (ZnSe, CdSe, PbSe) [31]. In these studies, methanol, ethanol, water, and CO_2 were used as solvents in the formation of sub- and super-critical fluids. Among them, alcohols exhibited greater advantages than water and CO_2 due to the more moderate conditions and simpler process. In addition, supercritical or subcritical alcohols technique could also be easily scaled up via a continuous flow type system [29, 35, 38, 39, 46].

To our knowledge, there is no report on the synthesis of cuprous oxide as the only product through sub- and supercritical alcohols. In this paper, we report a simple and scalable method for the synthesis of Cu_2O microcrystals with given morphologies in subcritical methanol by using inorganic copper salt as the precursor. Octahedral and cubic cuprous oxide microcrystals were obtained and applied as photocatalyst to degrade methyl orange. The influence of morphology on catalysis performance was also investigated.

Materials and methods

Synthesis of cuprous oxide

For solution feeding methods, typically, 4 g of $Cu(NO_3)_2{\cdot}3H_2O$ was dissolved in 30-mL methanol firstly and then introduced into a high-pressure tank reactor (150 mL) purged previously with nitrogen for several minutes. The system was heated to 200–250 °C within 15 min and kept for 15–30 min. In the process, the pressure of the system was 5.6–10 MPa. Upon the completion of the reaction, the reactor was immediately quenched with cold water. The precipitates were filtrated and washed with deionized water and methanol three times to remove the residues. Then, the products were dried in a vacuum oven for 24 h. All of the above reagents were purchased from Sinopharm Chemical Reagent Co, Ltd. (Shanghai, China) and were used without further purification.

For solid feeding methods, 4 g of $Cu(NO_3)_2{\cdot}3H_2O$ was introduced into the reactor firstly. After being tightly sealed, the air inside was replaced with N_2 for several minutes and then the N_2 was exhausted under vacuum for 10 min. 30-mL methanol was then discharged into the reactor. The reactor was heated to 230 °C within 15 min and kept for 15 min under the pressure of 7.8 MPa. Subsequent steps are the same with above process.

Characterizations

The particles were characterized by using XRD, SEM, and XPS. XRD patterns of the samples were conducted with an Empyrean X-ray generator (PANalytical B.V., Netherlands). The microscopic feature of the products was observed by scanning electron microscopy (SEM, S-4800 FESEM, Hitachi Ltd, Japan). X-ray photoelectron spectroscopy (XPS, ESCALAB250, Thermo VG, USA) was employed to analyze the surface of transition metal oxides powders.

Photocatalytic performance of cuprous oxide

To investigate the photocatalytic performance of the octahedral and cubic Cu_2O microcrystals, methyl orange (MO) (Sinopharm Chemical Reagent Co, Ltd.) was used as a model pollutant. The LED was used as a light source to provide irradiation. 0.1 g of the as-obtained cuprous oxide was dispersed in 100 mL of 10 mg/L aqueous methyl

orange solution in a quartz beaker. The solution was then stirred constantly under dark conditions for 60 min to ensure the adsorption/desorption equilibrium between MO and Cu_2O. The mixture was then irradiated with visible light irradiation under constant stirring for different time. 1 mL of the sample solution was withdrawn after irradiating at a certain intervals and taken to be detected by a UV–Vis absorption spectrometer (UV-5200, metash instruments Co, Ltd. Shanghai, China) after being treated typically.

Results and discussion

Characterization of synthesized samples

The XRD patterns as illustrated in Fig. 1 showed the crystal phase of samples synthesized in sub- and supercritical methanol with different temperatures and pressures for 30 min by using solution feeding method. All diffraction peaks in Fig. 1a could be indexed to the phase of CuO when the process was carried out under lower temperature (200 °C) and pressure (5.6 MPa). When the temperature and pressure were raised to 230 °C and 7.8 MPa, a mixture of CuO, Cu_2O, and Cu was obtained (Fig. 1b), while pure copper was formed under higher temperature (250 °C) and pressure (10 MPa) (Fig. 1c). The above results indicated that only moderate reaction condition (i.e., 230 °C, 7.8 MPa in Fig. 1b) was conductive to the formation of cuprous oxide. Moreover, Fig. 1b shows that there was a large amount of elemental copper, and only a small amount of Cu_2O in the mixture, which was supposed to be caused by long reaction time. Thus, the reaction time was shortened to 15 min by keeping the same moderate condition (230 °C, 7.8 MPa). Then diffraction peaks belonging to pure phase of cuprous oxide are observed in Fig. 2a, which could be well indexed to PDF 5-667 with the (224) *Pn-3 m* space group and $a = b = c = 4.27$ Å. Six peaks at $2\theta = 29.51$, 36.38, 42.22, 61.32, 73.48, and 77.26° corresponded to (110), (111), (200), (220), (311), (222) lattice planes of face-centered cubic (fcc) Cu_2O structure.

When solid feeding method (in Sect. 2.1) was adopted to synthesize cuprous oxide, pure cuprous oxide could also be obtained (see Fig. 2b) and all diffraction peaks were indexed to PDF 65-3288 with $a = b = c = 4.26$ Å. Interestingly, however, SEM results showed that the two Cu_2O samples synthesized by different feeding methods presented distinct morphologies as shown in Fig. 3. When solution feeding method was applied, the collected samples were octahedral Cu_2O with an edge length of 4 μm (Fig. 3a), and when solid feeding method was used, cubic Cu_2O with edge length of 2 μm was obtained (Fig. 3b).

The XPS was employed to analyze the surface composition of the Cu_2O product and the XPS spectrums of curve fitting of C 1s, N 1s, O 1s, and Cu 2p are shown as Fig. 4. The XPS spectrum was charge corrected to the adventitious C 1s peak at 284.6 eV. The C 1s peak was split into three peaks of 284.5, 285.4, and 287.9 eV, which were ascribed to elemental C, C–OH, and –C=O, respectively (Fig. 4a) [34], while the N 1s peaks in the spectra (see Fig. 4b) could be fitted into four peaks of 396.5, 398.1, 399.7, and 406.5 eV, which were ascribed to nitride, N–O, and NO_3^-, respectively [47, 48]. The O 1s peak could be fitted into 3

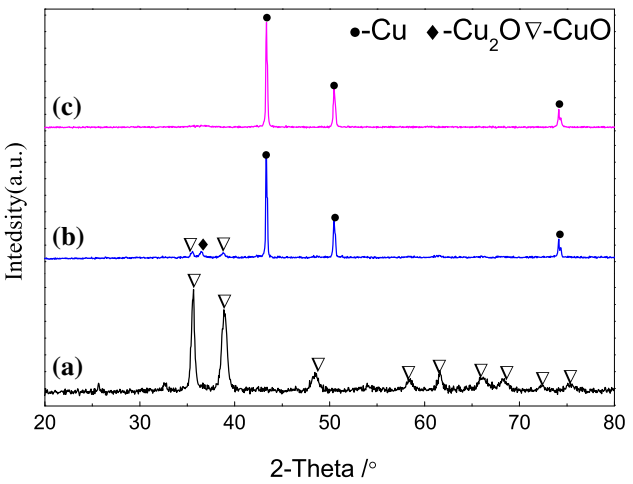

Fig. 1 XRD patterns of the products synthesized in sub- and supercritical MeOH for 30 min under **a** 200 °C, 5.6 MPa; **b** 230 °C, 7.8 MPa; **c** 250 °C, 10 MPa using solution feeding method

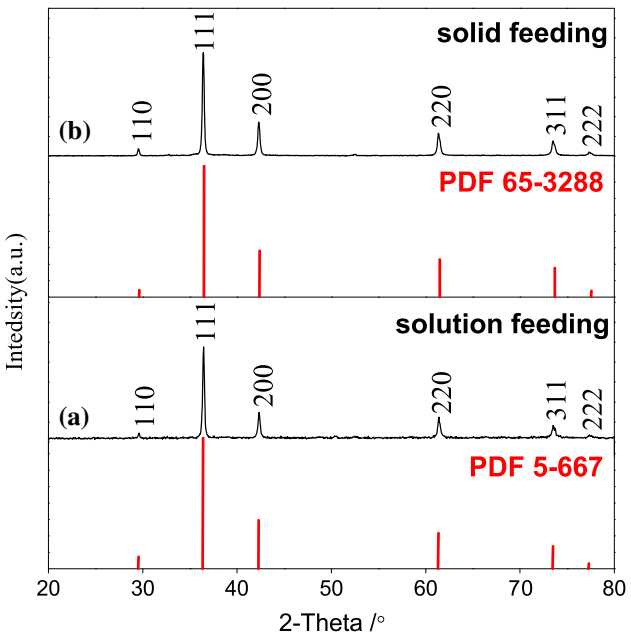

Fig. 2 XRD patterns of the cuprous oxide as synthesized in subcritical MeOH (230 °C, 7.8 MPa) for 15 min via **a** solution and **b** solid feeding methods

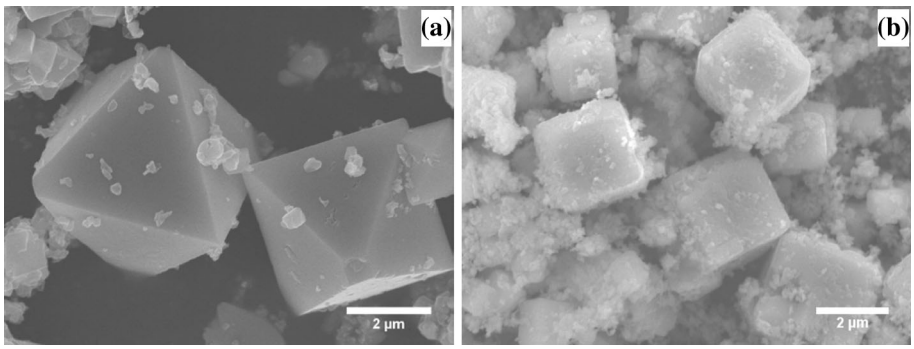

Fig. 3 SEM images of particles synthesized in subcritical MeOH (230 °C, 7.8 MPa) for 15 min via **a** solution and **b** solid feeding methods

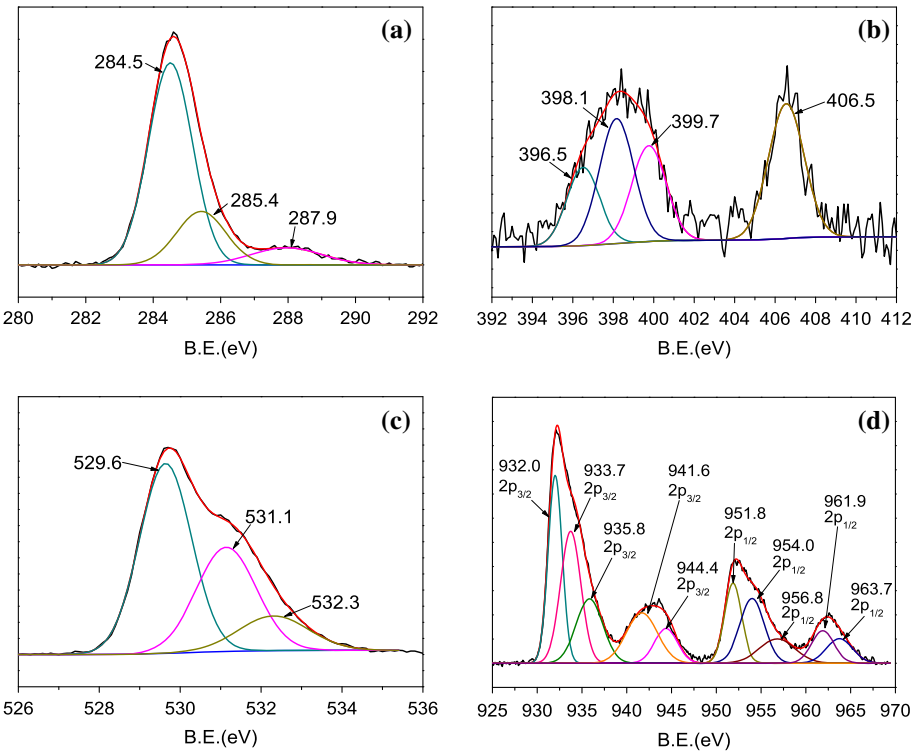

Fig. 4 XPS spectra of C 1s (**a**), N 1s (**b**), O 1s (**c**), and Cu 2p (**d**) peak fit in the as-prepared Cu_2O microcrystal

peaks. The peaks at 529.6, 531.1, and 532.3 were indexed to cupric oxide, cuprous oxide, and –C=O, respectively (Fig. 4c) [21, 34, 49]. In Fig. 4d, the two peaks located at 932.0 and 951.8 eV are assigned to Cu 2p in Cu_2O [21], and the six peaks at 933.7, 941. 6, 944.4, 954.0, 961.9, and 963.7 eV correspond to Cu 2p in CuO [49, 50], and peaks located at 935.8 and 956.8 eV are assigned to Cu 2p in $Cu(NO_3)_2$ [51]. Both O 1s peak (529.6 eV) and Cu 2p peak in CuO and $Cu(NO_3)_2$ indicated that there still was unreduced Cu^{2+} on the surface of the Cu_2O particles. In addition, the generation of –C=O group was confirmed by the peaks at 287.9 eV of C 1s and 532.3 eV of O 1s, which revealed that methanol was oxidized to formaldehyde in the process.

Proposed formation and crystal growth mechanism of Cu_2O

For further revealing the formation mechanism of cuprous oxide microcrystals in the subcritical methanol, the following proposed chemical reactions might be involved in the processes:

First, when reaching the subcritical domain, methanol was decomposed into free OH^- and CH_3^+, and copper nitride was decomposed into copper oxide, nitrogen dioxide, and oxygen, as described in Eqs. (1) and (2), respectively.

$$CH_3OH \rightarrow CH_3^+ + OH^- \quad (1)$$

$$2Cu(NO_3)_2 \rightarrow 2CuO + 4NO_2 + O_2 \quad (2)$$

Organometallic complex Cu(–O–CH_3)OH was synthesized as an intermediate via the collision of methyl cation, hydroxyl anion, and copper oxide. Then, electron transfer from oxygen atoms to copper atoms happened in the organ metallic complex to produce Cu^+–OH and methoxy radical (Eq. 3). In Eq. (4), electron was transferred from the O–H bond to O atom to produce Cu^+–O and H radical. Cu_2O and hydroxyl radical were then synthesized after the continuous electron transferring from Cu^+–O radical to Cu and O atom, as described in Eq. (5).

$$CH_3^+ + OH^- + CuO \longrightarrow HO\text{—}\overset{\frown}{Cu}\text{–}O\text{—}CH_3 \longrightarrow Cu^+\text{—}OH + \cdot OCH_3 \quad (3)$$

$$Cu^+\text{—}\overset{\frown}{O}\text{—}H \longrightarrow Cu^+\text{—}O\cdot + H\cdot \quad (4)$$

$$Cu^+\text{—}O\cdot \quad Cu^+\text{—}\overset{\frown}{O}\text{—}H \longrightarrow Cu_2O + \cdot OH \quad (5)$$

Subsequently, electron transfer in methoxy radicals produced formaldehyde and hydrogen radical (see Eq. 6). At the end of the process, hydrogen radical would react with hydroxyl radical formed in Eq. (5) and unreacted methoxy radical to produce water and methanol, as described in Eqs. (7) and (8).

$$\cdot O\text{—}CH_2\text{—}\overset{\frown}{H} \longrightarrow CH_2O + H\cdot \quad (6)$$

$$H\cdot + \cdot OH \rightarrow H_2O \quad (7)$$

$$H\cdot + \cdot OCH_3 \rightarrow CH_3OH \quad (8)$$

In addition, the formation mechanism of octahedral and cubic cuprous oxides could be explained according to the crystal growth theory [52], which believed that the morphology of monocrystal was determined by the relative growth rate of different crystal faces. Cu_2O belonged to the cubic crystal system, and the evolution of morphology mainly depended on the growth rate of {100} and {111} crystal plane [53]. When {111} facet grew relatively fast, Cu_2O crystal tended to form cubic, or else, it tends to form octahedron.

In this study, when solution feeding method was used, $Cu(NO_3)_2$ was dissolved adequately in methanol to release abundant NO_3^-, which would be adsorbed on the {111} facet of Cu_2O nucleation. This adsorption would prevent the crystal growth along the {111} facet, while {100} facet grew relatively faster. As a result, the stable {111} facets were preserved finally to form octahedron. While for solid feeding method, since the concentration of NO_3^- in methanol was lower, the growth of {111} facet of Cu_2O nucleation was faster than that of {100} facet, which resulted in the elimination of {111} facet and the formation of cubic Cu_2O finally.

Photocatalytic performance of cuprous oxides

Octahedral and cubic cuprous oxides were used as a photocatalyst for the decomposition of water containing methyl orange (MO), which was used as a model compound. For comparison, commercially available Cu_2O particles were used as control experiment. Figure 5 is the curves of the extent of photodegradation of MO vs. time for the two Cu_2O microcrystals as well as the control, dark and blank experiments. It was found that there was no decomposition for MO in dark in the presence of Cu_2O. Also no degradation was observed when the solution was placed under radiation but without Cu_2O. Moreover, there was also no apparent degradation when using bulk Cu_2O as catalyst in control experiment. As expected, both octahedron and cubic cuprous oxide microcrystal were much more photocatalytically active than bulk materials. The degrees of degradation of MO after 6 h of irradiation were 96.5 % and 92.1 % for octahedron and cubic, respectively. However, there was no significant difference in photocatalytic performance between octahedral and cubic. It suggested that in

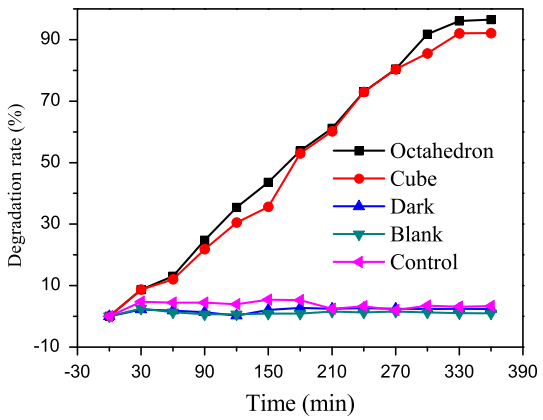

Fig. 5 Curves of the extent of photodegradation of MO versus. time for two Cu_2O microcrystals, the blank experiment did not contain Cu_2O crystals but only the methyl orange solution, the dark experiment was carried out without irradiation and the control experiment used commercially available Cu_2O as catalyst

the scale of micrometer (2–4 μm), morphology could not influence the photocatalytic performance.

Conclusion

Octahedral and cubic Cu_2O microcrystals with an average edge length of 4 and 2 μm, respectively, were synthesized by a simple and potentially scalable subcritical methanol method. It was concluded that pure phase of cuprous oxides could be obtained in a short reaction time (15 min) under moderate temperature (230 °C) and pressure (7.8 MPa). The feeding method played an important role in the formation process of different morphologies. The oxidation product, formaldehyde, was confirmed to exist on the surface of cuprous oxide, which suggested that the subcritical methanol acted as reaction medium as well as reducing agent in the process. In addition, both octahedron and cubic cuprous oxide microcrystal exhibited morphology-independent and excellent photocatalytic performance in the degradation of methyl orange.

Acknowledgements The authors gratefully acknowledge the financial supports by the Scientific Research Starting Foundation for Doctors of Science and Technology Agency of Liaoning Province, China (Grant No. 20111047) and (Grant No. 20121070), and Program for Liaoning Excellent Talents in University (Grant No. LR2012012) and (Grant No. LJQ2012034).

References

1. Ng CHB, Fan WY (2006) Shape evolution of Cu_2O nanostructures via kinetic and thermodynamic controlled growth. J Phys Chem B 110:20801–20807
2. Tsai YH, Chanda K, Chu YT et al (2014) Direct formation of small Cu_2O nanocubes, octahedra, and octapods for efficient synthesis of triazoles. Nanoscale 6:8704–8709
3. Chanda K, Rej S, Huang MH (2013) Investigation of facet effects on the catalytic activity of Cu_2O nanocrystals for efficient regioselective synthesis of 3,5-disubstituted isoxazoles. Nanoscale 5:12494–12501
4. Xu Y, Wang H, Yu YF et al (2011) Cu_2O nanocrystals: surfactant-free room-temperature morphology-modulated synthesis and shape-dependent heterogeneous organic catalytic activities. J Phys Chem C 115:15288–15296
5. Zhao Y, Wang W, Li Y et al (2014) Hierarchical branched Cu_2O nanowires with enhanced photocatalytic activity and stability for H_2 production. Nanoscale 6:195–198
6. Zhang L, Shi J, Liu M et al (2014) Photocatalytic reforming of glucose under visible light over morphology controlled Cu_2O: efficient charge separation by crystal facet engineering. Chem Commun 50:192–194
7. Feng L, Zhang C, Gao G et al (2012) Facile synthesis of hollow Cu_2O octahedral and spherical nanocrystals and their morphology-dependent photocatalytic properties. Nanoscale Res Lett 7:276
8. Hung L-I, Tsung C-K, Huang W et al (2010) Room-temperature formation of hollow Cu_2O nanoparticles. Adv Mater 22:1910–1914
9. Zhong JH, Li GR, Wang ZL et al (2011) Facile electrochemical synthesis of hexagonal Cu_2O nanotube arrays and their application. Inorg Chem 50:757–763
10. Guan L, Pang H, Wang J et al (2010) Fabrication of novel comb-like Cu_2O nanorod-based structures through an interface etching method and their application as ethanol sensors. Chem Commun 46:7022–7024
11. Shin JH, Park SH, Hyun SM et al (2014) Electrochemical flow-based solution-solid growth of the Cu_2O nanorod array: potential application to lithium ion batteries. Phys Chem Chem Phys 16:18226–18232
12. Paolella A, Brescia R, Prato M et al (2013) Colloidal synthesis of cuprite (Cu_2O) octahedral nanocrystals and their electrochemical lithiation. ACS Appl Mater Interfaces 5:2745–2751
13. Poizot P, Laruelle S, Grugeon S et al (2000) Nano-sized transition-metal oxides as negative-electrode materials for lithium-ion batteries. Nature 407:496–499
14. Sedighi A, Montazer M, Samadi N (2014) Synthesis of nano Cu_2O on cotton: morphological, physical, biological and optical sensing characterizations. Carbohydr Polym 110:489–498
15. Giannousi K, Sarafidis G, Mourdikoudis S et al (2014) Selective synthesis of Cu_2O and Cu/Cu_2O nps: antifungal activity to yeast saccharomyces cerevisiae and DNA interaction. Inorg Chem 53:9657–9666
16. Choi DJ, Maeng JS, Ahn KO et al (2014) Synthesis of Cu or Cu_2O -polyimide nanocomposites using Cu powders and their optical properties. Nanotechnology 25:375604
17. Li Q, Xu P, Zhang B et al (2013) Self-supported pt nanoclusters via galvanic replacement from Cu_2O nanocubes as efficient electrocatalysts. Nanoscale 5:7397–7402
18. Huang C, Ye W, Liu Q et al (2014) Dispersed Cu_2O octahedrons on h-BN nanosheets for p-nitrophenol reduction. ACS Appl Mater Interfaces 6:14469–14476
19. Xu H, Ouyang S, Liu L et al (2014) Porous-structured Cu_2O/TiO_2 nanojunction material toward efficient CO_2 photoreduction. Nanotechnology 25:165402
20. Huang WC, Lyu LM, Yang YC et al (2012) Synthesis of Cu_2O nanocrystals from cubic to rhombic dodecahedral structures and their comparative photocatalytic activity. J Am Chem Soc 134:1261–1267
21. Chanda K, Rej S, Huang MH (2013) Facet-dependent catalytic activity of Cu_2O nanocrystals in the one-pot synthesis of 1,2,3-triazoles by multicomponent click reactions. Chem Eur J 19:16036–16043
22. Ho JY, Huang MH (2009) Synthesis of submicrometer-sized Cu_2O crystals with morphological evolution from cubic to hexapod structures and their comparative photocatalytic activity. J Phys Chem C 113:14159–14164
23. Kuo CH, Huang MH (2008) Facile synthesis of Cu_2O nanocrystals with systematic shape evolution from cubic to octahedral structures. J Phys Chem C 112:18355–18360
24. Xu L, Jiang LP, Zhu JJ (2009) Sonochemical synthesis and photocatalysis of porous Cu_2O nanospheres with controllable structures. Nanotechnology 20:045605
25. Zhang H, Di Z, Zhang L et al (2009) Cu_2O hollow spheres: synthesis, characterization and magnetic property. J Nanosci Nanotechnol 9:1321–1325
26. Hacialioglu S, Meng F, Jin S (2012) Facile and mild solution synthesis of Cu_2O nanowires and nanotubes driven by screw dislocations. Chem Commun (Camb) 48:1174–1176
27. Ding Y, Ge D, Yang L et al (2013) Controllable synthesis of Cu_2O petalody octahedral microcrystals and multi-patterned evolution. J Colloid Interface Sci 392:151–157
28. Kim J, Kim D, Veriansyah B et al (2009) Metal nanoparticle synthesis using supercritical alcohol. Mater Lett 63:1880–1882

29. Choi H, Veriansyah B, Kim J et al (2010) Continuous synthesis of metal nanoparticles in supercritical methanol. J Supercrit Fluids 52:285–291
30. Shin NC, Lee YH, Shin YH et al (2010) Synthesis of cobalt nanoparticles in supercritical methanol. Mater Chem Phys 124:140–144
31. Pahari SK, Adschiri T, Panda AB (2011) Synthesis of monodispersed nanocrystalline materials in supercritical ethanol: a generalized approach. J Mater Chem 21:10377–10383
32. Desmoulins-Krawiec S, Aymonier C, Loppinet-Serani A et al (2004) Synthesis of nanostructured materials in supercritical ammonia: nitrides, metals and oxides. J Mater Chem 14:228–232
33. Gendrineau T, Marre S, Vaultier M et al (2012) Microfluidic synthesis of palladium nanocrystals assisted by supercritical CO_2: tailored surface properties for applications in boron chemistry. Angew Chem Int Ed 51:8525–8528
34. Yu S, Li S, Ge X et al (2014) Influence of reducing atmosphere of subcritical/supercritical mild alcohols on the synthesis of copper powder. Ind Eng Chem Res 53:2238–2243
35. Veriansyah B, Park H, Kim JD et al (2009) Characterization of surface-modified ceria oxide nanoparticles synthesized continuously in supercritical methanol. J Supercrit Fluids 50:283–291
36. Veriansyah B, Kim JD, Min BK et al (2010) Continuous synthesis of magnetite nanoparticles in supercritical methanol. Mater Lett 64:2197–2200
37. Veriansyah B, Chun MS, Kim J (2011) Surface-modified cerium oxide nanoparticles synthesized continuously in supercritical methanol: study of dispersion stability in ethylene glycol medium. Chem Eng J 168:1346–1351
38. Slostowski C, Marre S, Babot O et al (2012) Near- and supercritical alcohols as solvents and surface modifiers for the continuous synthesis of cerium oxide nanoparticles. Langmuir 28:16656–16663
39. Pascu O, Marre S, Aymonier C et al (2013) Ultrafast and continuous synthesis of crystalline ferrite nanoparticles in supercritical ethanol. Nanoscale 5:2126–2132
40. Li Z, Godsell JF, O'Byrne JP et al (2010) Supercritical fluid synthesis of magnetic hexagonal nanoplatelets of magnetite. J Am Chem Soc 132:12540–12541
41. Sue K, Suzuki M, Arai K et al (2006) Size-controlled synthesis of metal oxide nanoparticles with a flow-through supercritical water method. Green Chem 8:634–638
42. Rangappa D, Sone K, Ichihara M et al (2010) Rapid one-pot synthesis of $LiMPO_4$ (M = Fe, Mn) colloidal nanocrystals by supercritical ethanol process. Chem Commun (Camb) 46:7548–7550
43. Nugroho A, Kim SJ, Chang W et al (2013) Facile synthesis of hierarchical mesoporous $Li_4Ti_5O_{12}$ microspheres in supercritical methanol. J Power Sources 244:164–169
44. Nugroho A, Kim SJ, Chung KY et al (2011) Facile synthesis of nanosized $Li_4Ti_5O_{12}$ in supercritical water. Electrochem Commun 13:650–653
45. Hong SA, Kim SJ, Chung KY et al (2013) Continuous synthesis of lithium iron phosphate ($LiFePO_4$) nanoparticles in supercritical water: effect of mixing tee. J Supercrit Fluids 73:70–79
46. Hong SA, Kim SJ, Chung KY et al (2013) Continuous synthesis of lithium iron phosphate nanoparticles in supercritical water: effect of process parameters. Chem Eng J 229:313–323
47. Moulder J, Sticke W, Sobol P et al (1992) Handbook of X-ray photoelectron spectroscopy. Perkin Elmer Coorporation, Physical Electronics Division, USA
48. Baltrusaitis J, Jayaweera PM, Grassian VH (2009) XPS study of nitrogen dioxide adsorption on metal oxide particle surfaces under different environmental conditions. Phys Chem Chem Phys 11:8295–8305
49. Zarate RA, Hevia F, Fuentes S et al (2007) Novel route to synthesize CuO nanoplatelets. J Solid State Chem 180:1464–1469
50. Zheng Z, Huang B, Wang Z et al (2009) Crystal faces of Cu_2O and their stabilities in photocatalytic reactions. J Phys Chem C 113:14448–14453
51. Shen JS, Chen YL, Wang QP et al (2013) In situ synthesis of red emissive copper nanoclusters in supramolecular hydrogels. J Mater Chem C 1:2092–2096
52. Rawlings JB, Miller SM, Witkowski WR (1993) Model identification and control of solution crystallization processes: a review. Ind Eng Chem Res 32:1275–1296
53. Wang ZL (2000) Transmission electron microscopy of shape-controlled nanocrystals and their assemblies. J Phys Chem B 104:1153–1175